Journal of Alloys and Compounds 1015 (2025) 178895

Contents lists available at ScienceDirect

Journal of Alloys and Compounds

journal homepage: www.elsevier.com/locate/jalcom

Optimized $Bi_4Si_3O_{12}$ scintillation crystals grown in dynamic atmosphere for future particle physics experiments

S. Tkachenko [a], I. Gerasymov [a], D. Kurtsev [a], O. Viahin [a], D. Kofanov [a], B. Grynyov [a], P. Mateychenko [b], E. Bryleva [c], L. Martinazzoli [d,e], J. Delenne [d,f], L. Roux [d,g], R. Cala' [d], E. Auffray [d], O. Sidletskiy [a,h,*]

[a] Institute for Scintillation Materials NAS of Ukraine, Kharkiv, Ukraine
[b] Institute for Single Crystals NAS of Ukraine, Kharkiv, Ukraine
[c] State Scientific Institution "Institute for Single Crystals" NAS of Ukraine, Kharkiv, Ukraine
[d] European Organization for Nuclear Research (CERN), Geneva, Switzerland
[e] INFN & Università degli Studi di Milano-Bicocca, Milan, Italy
[f] Université de Strasbourg, UMR 7178 CNRS, IPHC, Strasbourg, France
[g] Université Claude Bernard Lyon1, UMR5306 CNRS, ILM, Lyon, France
[h] Centre of Excellence ENSEMBLE3 Sp. z o.o., Warsaw, Poland

ARTICLE INFO

Keywords:
Bismuth silicate
Scintillator
Particle physics
Growth atmosphere
Crystal growth
Czochralski method

ABSTRACT

This work deals with the optimization of bismuth silicate, $Bi_4Si_3O_{12}$ (BSO) scintillation crystals as candidates for future high energy physics experiments at colliders involving the registration of both scintillation and Cherenkov light. Crystals with a high transparency in UV-band and a high timing resolution are required for this application. Czochralski process was employed for BSO crystal growth in Pt crucibles in a dynamic growth atmosphere. After the growth of a series of crystals in air, as well as mixed Ar-air static and dynamic atmospheres, it was shown that the mixed atmosphere minimizes Bi_2O_3 evaporation and reduces the amount of Pt dissolved in the melt by several times. This caused the reduction in the number of foreign inclusions in the grown crystals, providing a transparency of over 70 % in the $>$ 300 nm range, a light output of up to 2140 ph/MeV, an energy resolution of 21.5 % at 662 keV γ-rays, while a coincidence time resolution was improved from 148 to 125 ps.

1. Introduction

$Bi_4Ge_3O_{12}$ (BGO) scintillator has been widely used in particle physics experiments because of its high density, short radiation length, and relatively high light output of about 8000 ph/MeV [1,2]. However, this crystal possesses a slow decay time of 300 ns and moderate radiation hardness, which limits its application in experiments where fast timing and high radiation hardness are crucial. On the other hand, bismuth silicate, $Bi_4Si_3O_{12}$ (BSO) having the same crystal structure as BGO, seems to be a possible alternative, because of its shorter decay time of 100 ns and better radiation hardness, although a lower light output of 1600 ph/MeV [4]. In addition, a blue-shift of the BSO transmission cut-off with respect to BGO allows a wider range of wavelengths for extracting Cherenkov radiation. Meanwhile, $Bi_4Ge_{3-x}Si_xO_{12}$ (BGSO), a BGO-BSO solid solution, combines a moderate light yield with a fast scintillation rise/decay and is an efficient Cherenkov radiator, as was demonstrated [5]. These features are promising for the development of dual-readout detectors for registration of both scintillation and Cherenkov signals and potentially advantageous in terms of fast timing due to very fast decay of Cherenkov radiation [1–3,5]. However, BGSO growth process is complicated, yielding a lot of inclusions in crystals related to non-uniform distribution of the Ge- and Si-enriched components in the solid solution. This is caused by a large difference in ionic radii of Si^{4+} and Ge^{4+} substitutional ions (32 %), out of the solubility threshold (15 %) according to the Holdshmidt's rule.

BSO crystals are grown mainly by the Bridgman and Czochralski methods [6–9]. Both methods have their advantages and disadvantages in relation to this material. In the Bridgman method, gaseous impurities and light foreign phases are pushed by gravitational force upwards to the melt surface from the crystallization interface. In contrast, in the Czochralski method, admixtures in melt accumulate at the melt surface near the crystallization interface and can be captured by the crystal. The

* Correspondence to: Institute for Scintillation Materials NAS of Ukraine, Kharkiv, Ukraine.
E-mail addresses: sidletskiy@isma.kharkiv.ua, oleg.sidletskiy@ensemble3.eu (O. Sidletskiy).

https://doi.org/10.1016/j.jallcom.2025.178895
Received 29 November 2024; Received in revised form 4 January 2025; Accepted 27 January 2025
Available online 28 January 2025

main disadvantages of the Bridgman method are the impossibility of monitoring and direct controlling the crystal growth rate, and complicated melt homogenization as usually ampoule (crucible) rotation is not provided. Additionally, crystals stick to the ampoule, making unloading the crystal difficult. For these reasons, the Czochralski method looks preferable to grow large BSO crystals.

A specific problem of growing BSO crystals is a high reactivity of their components, silicon oxide (SiO_2) and bismuth oxide (Bi_2O_3) which can be melted only in iridium or platinum crucibles [10,11]. Meanwhile, even platinum may be dissolved by Bi_2O_3-containing melt owing to a high chemical activity of the latter [10–12], herein Pt solubility is proportional to Bi_2O_3 concentration in the melt [11]. Bismuth oxide heated to 210 °C in an oxygen-containing atmosphere oxidizes to the Bi_2O_5 higher oxide [13], while Bi_2O_5 reduces back to the trivalent state with the release of oxygen in the temperature range of 210 – 660 °C. Bismuth oxide acts as a source of oxygen that oxidizes platinum at these temperatures. Silicon oxide (SiO_2) promotes platinum dissolution as well. The solubility of Pt in silicate glasses reaches 20 ppm at 1500 °C [14]. Herein, Pt solubility in a $Bi_4Si_3O_{12}$ melt is strongly dependent on melt temperature: upon increasing the temperature from 1050 °C to 1300 °C the concentration of dissolved platinum doubles from 20 to 40 ppm [12], hence melt overheating is highly undesirable.

This work is focused on optimization of optical and scintillation performance of BSO crystals for future particle physics experiments grown by the Czochralski method in Pt crucibles by creating dynamic atmosphere composition and minimization of Bi_2O_3 evaporation and Pt losses.

2. Experimental

2.1. Crystal growth

BSO crystals were grown by the Czochralski method in an inductively heated platinum crucible of 58 mm in diameter and 53 mm in Al_2O_3 ceramic thermal insulation. Crystal growth was carried out in air and Ar-air atmospheres. The growth rate was 1 mm/h. Bi_2O_3 and SiO_2 powders with a purity of 99.999 % were used as raw materials. Pre-dried powders were mixed and sintered in air in a platinum crucible at a temperature of 850 °C for 6 hours. To estimate the amount of platinum loss, the crucible was cleaned and weighed before and after the growth process.

2.2. Determination of structure and admixture content

The powder diffraction measurements were carried out by Siemens D500 diffractometer, CuKα radiation, Bragg–Brentano geometry, curved graphite monochromator on the counter arm, $5° < 2\theta° < 100°$, and $\Delta 2\theta = 0.02°$. The phases were identified using JCPDS PDF-1 card files and EVA retrieval system included in the diffractometer software.

The morphology and elemental composition of the sample surfaces were controlled by a JSM-6390LV scanning electron microscope (SEM) with the AZtechEnergy X-max^n 50 microanalysis system (EDS). The platinum content in bismuth silicate was determined using inductively coupled plasma atomic emission spectrometry (ICP-AES). A weighed portion of the sample was placed in a glassy carbon crucible, followed by the addition of 10 mL of HF, 5 mL of HCl, and 2 mL of HNO_3. The crucible was then covered with a PTFE lid and heated on an electric hot plate at the minimum temperature required for complete dissolution. After dissolution, the solution was cooled to room temperature, transferred to a polyethylene volumetric flask, and diluted to the mark with a 10 % aqueous HCl solution. Platinum concentrations were measured using an iCAP 6300 Duo spectrometer (Thermo Corporation, USA), equipped with a PTFE sample introduction system. The analysis was performed under standard operating conditions using the method of standard additions, with the 265.945 nm analytical line for Pt.

2.3. Optical and scintillation characterization

Transmission spectra of the samples were measured using a PerkinElmer LAMBDA 650 UV/VIS spectrometer. The instrument provided with a deuterium and halogen lamp and covers the wavelength range of 190–900 nm. The light passes through a monochromator and then split into two branches. One of the monochromatic light beams, whose intensity can be tuned by means of an iris, traverses the crystal sample placed on a moving stage. The other beam is instead employed to monitor instrumentation drift during the acquisition. Both beams are focalized through a photomultiplier measuring their intensity. The samples for transmission measurements were fabricated from the upper parts of the crystal cones, which are visually the most transparent and do not contain inclusions.

The pulse-height spectra of the samples were measured using a setup consisted of a Hamamatsu R2059 PMT, analog attenuator and DT5720 CAEN digitizer working in charge integration mode. The crystals were placed directly to input window of PMT with Rhodorsil grease coupling and wrapped with Teflon to maximize light collection. The ^{137}Cs (662 keV) gamma radioactive source was used for excitation of scintillations. The whole setup was enclosed in a temperature controlled black box. The PMT is biased at 2500 V, providing sufficient gain to resolve the charge of single photoelectron pulses, that allows to convert the total charge of a scintillation event to photoelectrons produced. The number of photons impinging on the PMT (light output) is obtained correcting for the quantum efficiency of the PMT, convolved with the emission spectra of the samples.

The scintillation decay curves were measured using a Time Correlated Single Photon Counting (TCSPC) setup [15]. A pulse diode laser (Pico-Quant, PDL 800-B) was used as an excitation source of an X-ray tube XRT N5084 from Hamamatsu. It generated an X-ray beam with a continuous energy spectrum between 0 and 40 keV (with a $\simeq$ 10 keV mean energy). The beam, after crossing a brass collimator, was focused on the tested sample and its scintillation light was collected using a hybrid photomultiplier (HPM 100–07 Becker Hickl) working in TCSPC mode. A 420 nm long pass filter was placed in front of the hybrid photomultiplier to suppress air excitation contribution to the emission distributions. The measurements were done hitting the sample on one surface and detecting the emitted light from the same surface (reflection mode). The signal of the hybrid PMT was then fed to an amplifier and timing discriminator and was then used as the stop signal of a time to digital converter, while the start was provided by an external trigger of the pulse diode laser. Scintillation time profile for each sample was mathematically described with a multi-exponential function:

$$f(t) = \sum_{i=1}^{3} R_i \frac{\exp\left(-\frac{t-\theta}{\tau_{d,i}}\right) - \exp\left(-\frac{t-\theta}{\tau_r}\right)}{\tau_{d,i} - \tau_r} \Theta(t-\theta) + bkg \quad (1)$$

where $\tau_{r,i}$ and $\tau_{d,i}$ are the i-th components of the rise and decay time constants respectively, while ρ_i is the weight of the i-th component, θ is the instant above which the scintillation pulse starts and ε is the background. The scintillation pulse function defined above was then convoluted with the instrumental response function (IRF) of the setup ($\simeq$ 160 ps FWHM) to fit the decay spectra obtained. Then, the effective decay time was defined as:

$$\frac{1}{\tau_{d,eff}} = \sum_{i=1}^{3} \frac{A_i}{\tau_{d,i}} \quad (2)$$

The coincidence time resolution (CTR) is defined as the resolution of the difference in detection time of two 511 keV back-to-back gamma photons produced by a ^{22}Na source. The CTR were measured at CERN with dedicated setup exploiting high-frequency electronics for SiPMs readout and is described early in detail in [16]. A ^{22}Na source was placed between the $2 \times 2 \times 3$ mm^3 BSO sample under study and a reference

$2 \times 2 \times 3$ mm^3 BGO sample from Epic. Both the measured and reference samples were wrapped in several layers of Teflon and coupled to two Broadcom NUV-HD-MT 4×4 mm^2 SiPMs (30 μm SPAD size, powered at 48 V) with Cargille Meltmount optical glue. Metal-filled trenches (MT) were placed around the single-photon avalanche diodes in the state-of-the-art NUV-MT SiPM.

3. Results and discussion

3.1. BSO growth in the air atmosphere

Interaction of Pt with BSO melt and growth atmosphere is harmful not only from the point of a decreased crucible lifetime. Additionally, Pt inclusions on the crystal surface initiate cracks. The conditions of Pt interaction with oxygen during heating were addressed in [17]. Oxygen forms chemisorbed layers on the Pt surface, and Pt oxidizes when heated in air. The oxidized layer consists of a mixture of PtO, Pt_3O_4 and PtO_2 oxides., while the oxidation rate is limited by the diffusion rate of oxide molecules through the metal boundary layer. Evaporation of the oxidized layer begins above 450 °C, and above 800 °C it completely disappears.

Bismuth oxide evaporates from the BSO melt because the Bi_2O_3 vapor pressure is higher than that of SiO_2 at high temperatures. In our experiments, up to 2 g of Bi_2O_3 evaporated from 590 g of the melt during 170 hours of crystal growth, which is 0.4 wt% of the loaded Bi_2O_3, was deposited on the growth chamber walls and cold parts of the ceramic thermal insulation. The deposit consisted of 31 % bismuth and 69 % oxygen, with no silicon detected. This may indicate that above the BSO melting temperature of 1050 °C the processes of interaction between the melt and crucible are affected predominantly by the dissociation of bismuth oxide, rather than silicon oxide.

A series of BSO crystals were grown in our experiments. The platinum crucible lost 0.30 ± 0.02 g on average during the crystal growth in air atmosphere. The losses were caused by both evaporation of platinum from the free crucible surface, and dissolution of platinum into the melt. To distinguish the contributions from these factors, the empty crucible was heated to temperature similar to the conditions of the crystal growth process. The crucible without melt lost 0.224 g, thus, the presence of 590 g of BSO melt increased the platinum losses by 0.076 g. At the same time, the Pt concentration in the melt reached 0.013 wt% (Table 1). Despite the absolute values of Pt loss are not so high, it calls significant crucible damage. Furthermore, Pt dissolved in the melt and then deposited on the crystal surface call cracks in the latter due to the difference in thermal expansion coefficient between BSO and Pt.

As mentioned in Introduction, a surface layer of a platinum crucible oxidizes in air at temperatures up to 450 °C, while evaporation and dissociation of platinum oxide occurs at higher temperatures. In our experiments, it was observed that a metallic Pt deposited from the gas phase was observed on the ceramic thermal insulation in the form of dendrites (Fig. 1) with a length of up to 1 mm as a result of platinum oxide dissociation.

Particles of metallic Pt were observed on the surface of all grown crystals (Fig. 2a-c). Pt inclusions had a characteristic hexagonal or triangular shape (Fig. 2d) evidencing their monocrystallinity. The average size of platinum crystals was 40–60 μm, and the maximum one was 125 μm. Platinum grains were uniformly distributed along the entire crystal surface and had the same size at the top and bottom parts of the crystal. This became possible only if the Pt deposition rate was uniform during the entire crystal growth process. Deposition and crystallization of Pt from the gas phase can be excluded, as in this case the grain size in the upper part of the crystal would be larger because it was in contact with the gas during much longer period of time. Additionally, as demonstrated in Fig. 1, Pt dendrites are formed during crystallization from the gas phase, in contrast to what we observed on the crystal surface in Fig. 2.

Platinum deposition started immediately after crystal seeding, and, as the crystal grew, Pt dissolved in the BSO melt crystallized uniformly along the surface. Evidently, a dynamic equilibrium was formed between the rates of Pt dissolution in the BSO melt and its deposition on the crystal surface when the Pt concentration in the melt reached saturation. Additionally, decrease in the amount of melt also contributed to supersaturation. By the end of the crystal growth process, the platinum concentration in the remaining melt was 0.019 wt%. Additionally, the crystal was colored due to the presence of color centers and inclusions (Fig. 3a,b). To determine the nature of these inclusions, the crystallized melt remained in the crucible was characterized by XRD. Apart of the main eulitine phase of $Bi_4Si_3O_{12}$ with the 87 % content, 13 % of $Bi_{12}SiO_{20}$ sillenite phase was discovered (Fig. 4).

Table 1
Platinum losses under different growth atmospheres.

Composition of gas atmosphere	Pt loss, g		Pt concentration, wt%	
	Crucible with raw material	Crucible without raw material	in melt*	in crystal
Air (before the process starts)	0.3	0.224	$13 \cdot 10^{-3}$	$< 3 \cdot 10^{-4}$
Ar + air (before the process starts)	0.106	0.056	$8.5 \cdot 10^{-3}$	$< 3 \cdot 10^{-4}$
Ar (before the process starts), Air (after T > 600 °C)	0.066	0.034	$5.5 \cdot 10^{-3}$	$< 3 \cdot 10^{-4}$

*calculated data assuming that all reacted Pt remained in the melt or on the crystal surface

3.2. Growth in the static Ar-air atmosphere

In order to reduce the dissolution of platinum, crystal was grown in a mixed Ar-air atmosphere keeping all other conditions the same as at growth in air (Fig. 3c). As one may see, in the upper part the crystal became visually transparent, without coloration. The crucible lost 0.106 g, which is almost three times less than when growing in air (see Table 1). A decrease in the oxygen concentration in the chamber atmosphere reduced the platinum oxidation, as well as PtO_2 evaporation from the crucible surface and PtO_2 dissolution in the BSO melt. Note that dissolving of platinum oxide in the melt and the subsequent reduction of metallic platinum on the crystal surface occurred mainly at the very beginning of the crystal growth process (see Fig. 3c). Meanwhile, surface inclusions of Pt on the main part of the crystal were much smaller in size, ca. 5 μm (Fig. 5e,f), and their density over the area was remarkably smaller (Fig. 5a). A decrease of the oxygen partial pressure in the growth chamber atmosphere accelerated the dissociation of PtO_2 and release of metallic platinum. Rapid decomposition of PtO_2 led to the formation of a spongy metal texture (Fig. 5c,d) on the crystal neck surface. Several pieces of spongy platinum, 250 μm in size, grew into the crystal at the cone part, which is unlikely at crystallization from the gas phase.

After heating the empty crucible in an Ar-air atmosphere to temperature of BSO crystal growth, the weight loss was 0.056 g, whereas when crucible is heated with the melt, the loss reached 0.106 g (see Table 1). Thus, the contribution of the melt to the platinum loss was 0.050 g, and almost all Pt was deposited on the crystal neck. The platinum concentration in the crystal was below $3 \cdot 10^{-4}$ wt%, indicating the lower Pt loss at lower the oxygen concentration in the chamber atmosphere. The above results confirm that the growth of a BSO crystal in pure Ar atmosphere is undesirable, since in the absence of oxygen the dissociation of bismuth oxide and its evaporation increase, shifting the melt composition from the stoichiometry.

3.3. Growth in the dynamic Ar-air atmosphere

Since platinum is oxidized in the temperature range up to 450 °C

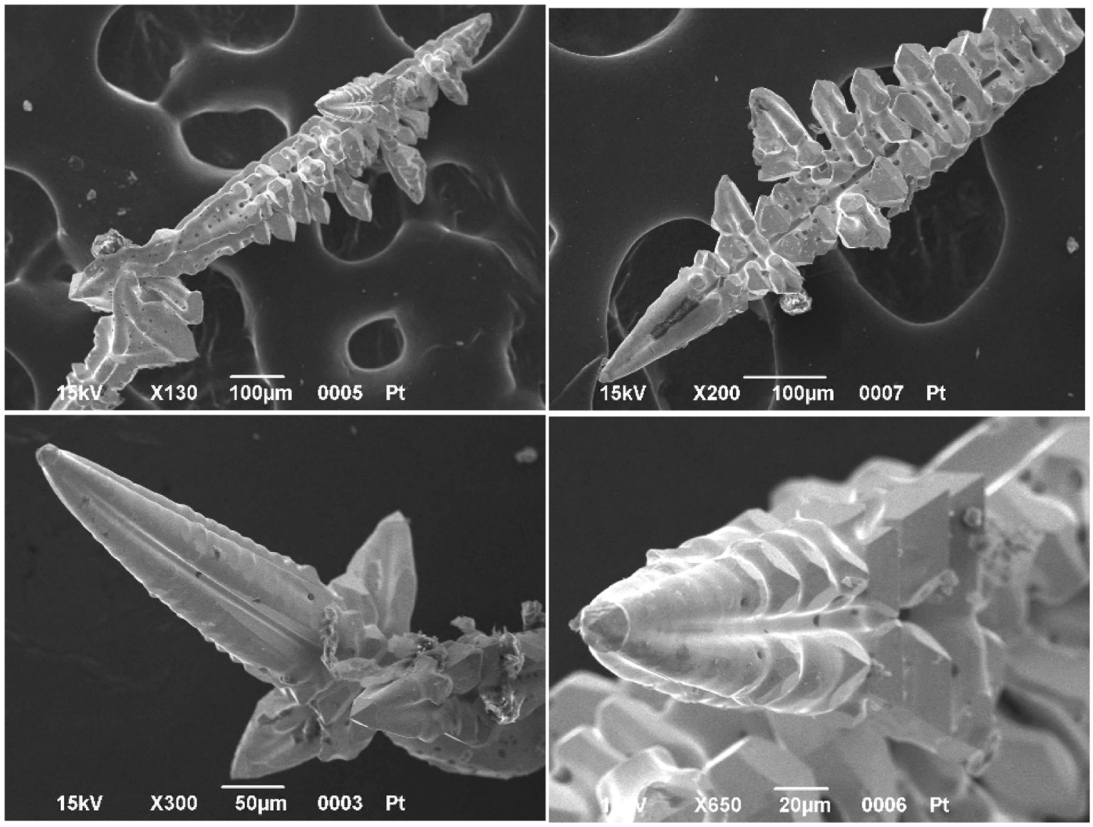

Fig. 1. Platinum dendrites deposited on heat insulation ceramics.

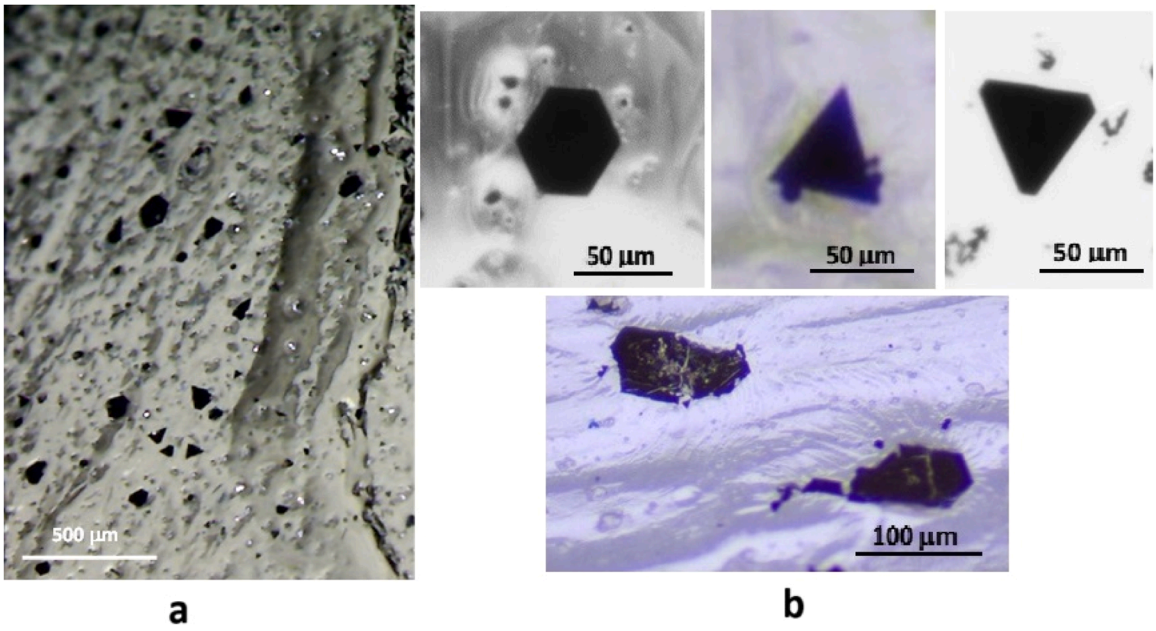

Fig. 2. SEM images of inclusions of metallic platinum on the surface of a BSO crystals grown in air atmosphere (a); monocrystalline Pt grains of different shape on the surface of the crystal grown in air (b).

[16], a series of experiments were conducted with dynamic gas atmosphere in the growth chamber. The growth chamber was evacuated with a forevacuum pump and filled with Ar up to 0.2 atm pressure. Then the empty crucible was heated to a temperature of 600 °C, and the chamber was additionally filled with air. As a result, the platinum loss further decreased to 0.034 g (see Table 1). A photo of a crystal grown in Ar-air dynamic atmosphere is presented in Fig. 3d. Crystal surface contained few Pt deposits, even less compared to growth in Ar+air static atmosphere, see the photos in Fig. 5a and b.

From our previous experience of work with molybdenum and tungsten crucibles for crystal growth [18,19] it is known that porous aluminum oxide and zirconium oxide ceramics absorbs a large amount

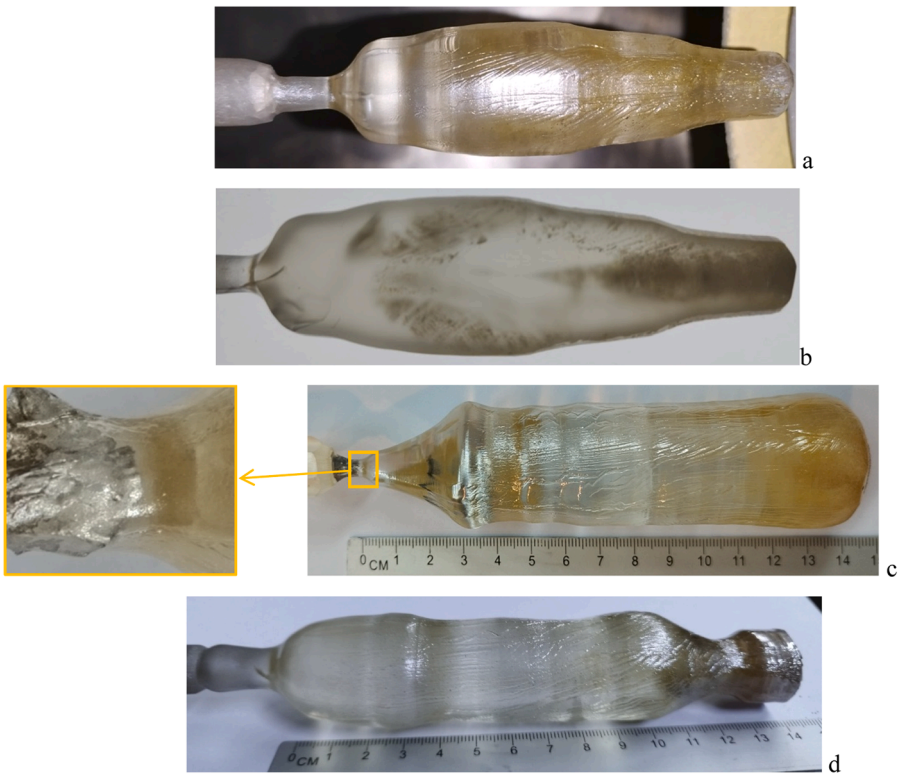

Fig. 3. BSO crystal grown in Air atmosphere (a) and its transverse cut (b), BSO grown in static Ar-air atmosphere (c) and dynamic Ar-air atmosphere (d). The inset in (c) represents the enlarged photo of the seed part covered with Pt.

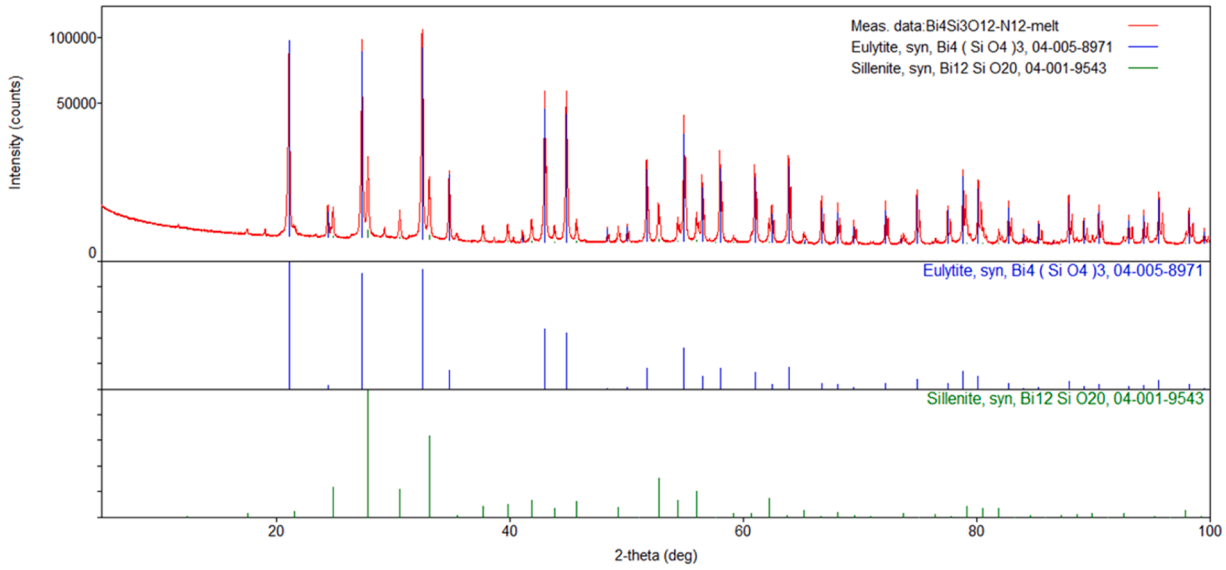

Fig. 4. X-ray diffractograms of crystallized melt after BSO crystal growth in air atmosphere.

of oxygen, which oxidizes a Mo crucible during heating. Our present experiments in this work with sequential filling the chamber with argon and then air demonstrated that Pt parts may be oxidized as well by oxygen accumulated in the heat insulation ceramics. Moreover, the surface of the crucible was partially oxidized when temperature decreased after completion of the crystal growth, i.e., crucible surface already contains an oxide layer when the crucible is reused. Therefore, it would not be possible to completely eliminate platinum losses. By growing the crystal in an Ar environment with air introduced into the chamber after heating the argon to 600 °C, it was possible to reduce the total loss of platinum to 0.066 g (see Table 1), which is 4 times less than when grown in air.

3.4. Optical and scintillation parameters

The decrease in Bi_2O_3 evaporation and Pt losses is reflected in the optical and scintillation parameters of the crystals. In Fig. 6a, the transmission spectra of BSO grown in air and in dynamic Ar-air atmosphere are presented. It can be seen that the crystal grown in the mixed atmosphere has improved transmittance. Inset in Fig. 6a demonstrates

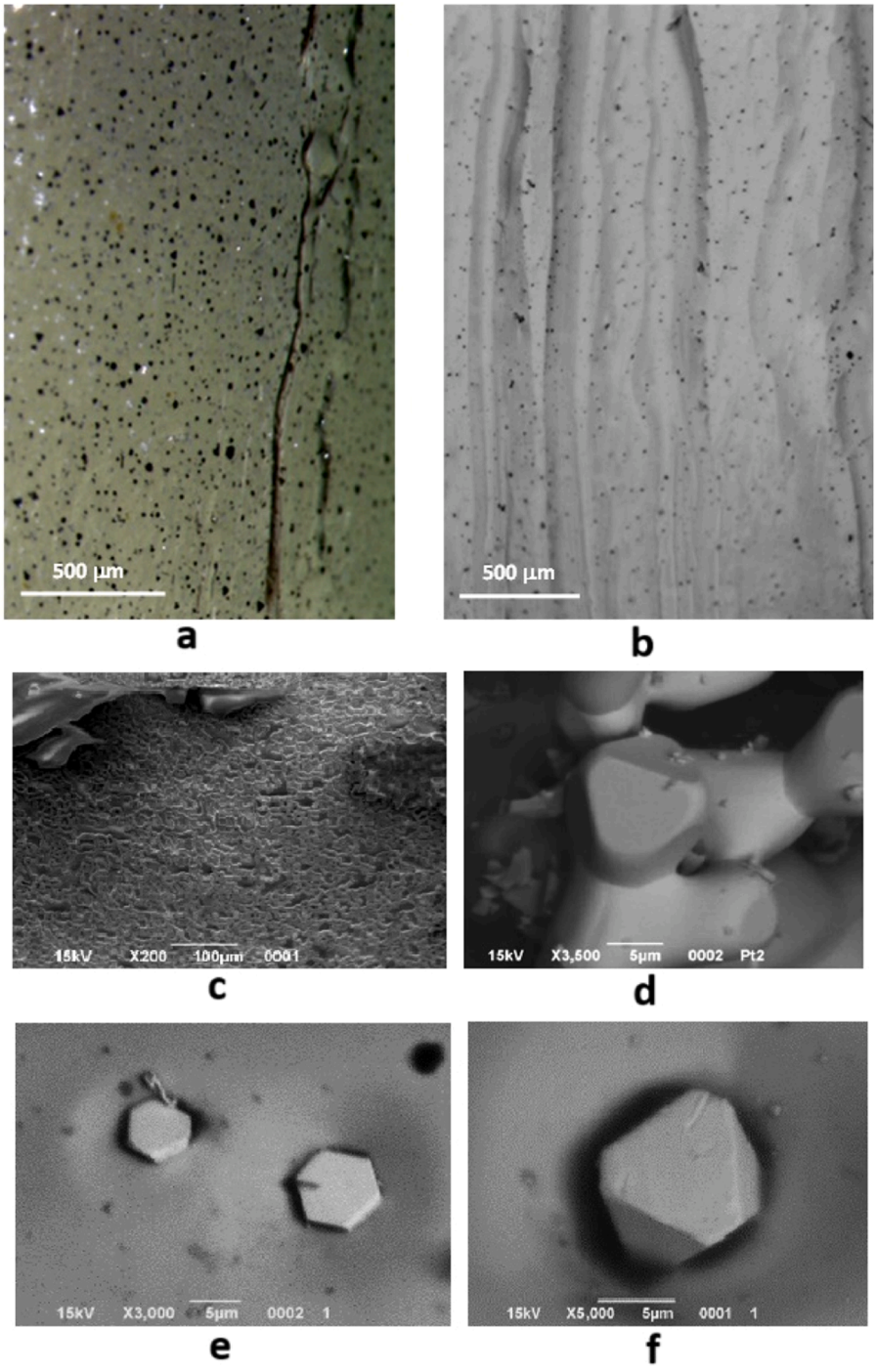

Fig. 5. SEM images of metallic platinum on the surface of a crystal grown in Ar-air atmosphere (a) and dynamic growth atmosphere (b). Spongy structure on the neck of the crystal grown in Ar-air atmosphere (see Fig. 3b) with different magnifications (c, d), and Pt microcrystals on the side surface of the same crystal (e, f).

enlarged spectra near the short-wavelength transmission edge.

Fig. 6b presents the BSO air transmission spectrum subtracted from the BSO Ar-air spectrum. The spectrum involves a low-intensity band peaked around 550 nm, as well as more intense, broad unresolved band extending from 330 nm to 450 nm. At present, there are relatively few experimental studies on the nature of color centers in $Bi_4Si_3O_{12}$ crystal host. However, computer modeling of BSO band structure indicates that the main intrinsic defects in such crystals are oxygen-related defects of Frenkel, Schottky and anti-Schottky types [20,21]. According to [20], the formation energies of these defects are 5.21 eV, 7.79 eV and 10.53 eV, respectively. On the other hand, intrinsic defects involving Bi^{3+} and Si^{4+} in interstitial positions have much higher formation energies, in contrast to bismuth germanate, $Bi_4Ge_3O_{12}$, where Bi antisite is the most energetically favorable defect [22]. Evidently, this is because the Ge^{4+}ionic radius is significantly larger compared to Si^{4+} one, allowing Bi^{3+} ions to replace Ge^{4+} in BGO more easily than Si^{4+} in BSO crystals.

Although we cannot assign the absorption bands in the subtracted spectrum to certain defect types, it is clear that transmission of BSO crystals grown under the optimized dynamic atmosphere is improved compared to the BSO grown in air. Importantly, the transmission window is extended in the UV that enables better transmission of Cherenkov radiation in UV (see the inset in Fig. 6a).

Fig. 7a,b presents the typical pulse-height spectra as well as the

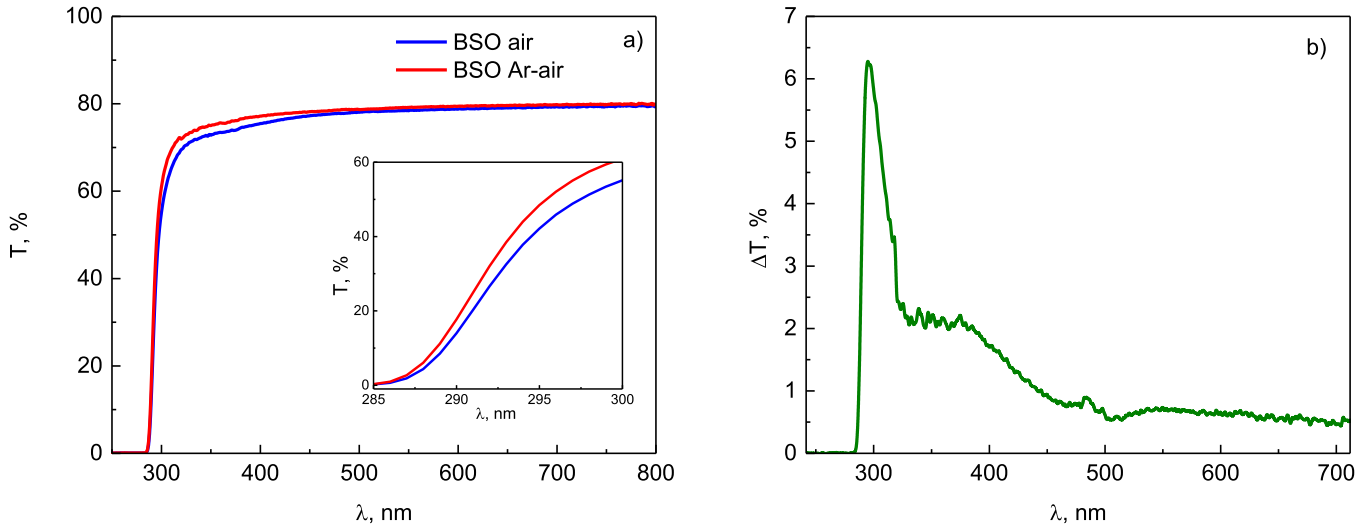

Fig. 6. Transmission spectra of BSO grown in air atmosphere and Ar-air dynamic atmosphere (a); the difference of the two transmission spectra (b). The inset in (a) represents the transmission spectra in the wavelength region near the transmission window edge.

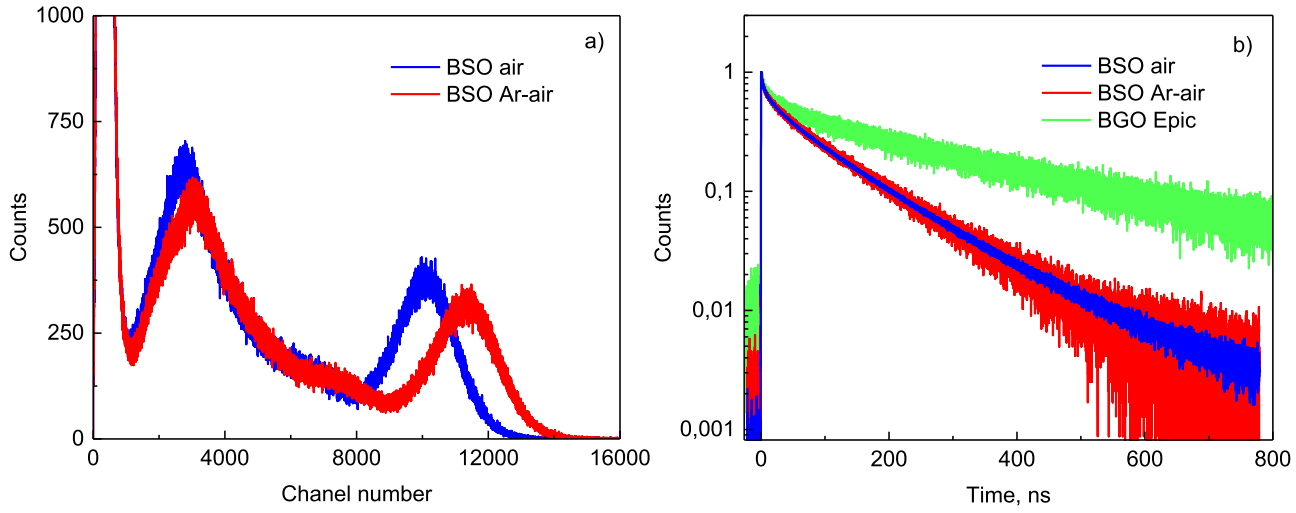

Fig. 7. Pulse-height spectra (a) and scintillation decay curves (b) of BSO crystals growth in different atmospheres in comarison with BGO reference obtained from Epic.

decay curves of crystals grown in different atmospheres. Crystals grown in the dynamic atmosphere exhibit improved scintillation parameters – a light output of 2140 ph/MeV vs. 1900 ph/MeV and an energy resolution at 662 keV of 21.5 vs. 23 % respectively (Fig. 7a). These parameters are superior compared to the literature where the light yield of ca. 1600 ph/MeV (20 % of BGO) [6], ca. 2000 ph/MeV (25 % of BGO) [23], and ca. 2100 (26 % of BGO) [24] were reported, and the energy resolution was 32 % [6], 24.87 % [23], and 22 % [24] for undoped BSO. The decay curves measured under pulsed X-ray excitation and corresponding effective decay constants are similar for crystals grown in the different atmospheres (Fig. 7b and Table 2) and give the effective decay times around 71 ns (against 74 ns [23] in literature), and the rise times of 13 and 21 ps. Nevertheless, the CTR value in the BSO sample grown in the dynamic atmosphere was improved to 125 ps (Fig. 8, Table 2), evidently, due to a wider transmission window favorizing Cherenkov detection and a higher light output.

4. Conclusions

Large BSO crystals with diameter up to 30 mm and cylindrical part length up to 100 mm with optimized optical transmission and scintillation performance were obtained by the Czochralski method. Factors

Table 2
Decay time components and coincidence time resolution (CTR) of the BSO crystals grown in different atmospheres.

Crystal	τ_r [ps]	τ_{d1} [ns]	τ_{d2} [ns]	τ_{d3} [ns]	A_1 [%]	A_2 [%]	A_3 [%]	$\tau_{d,eff}$ [ns]	CTR FWHM NUV-HD-MT SiPM [ps]
BGO (Epic)	85	3.36	22.54	287.68	0.43	3.34	96.23	163.71	143 ± 5
BSO air	13	4.83	45.82	133.73	2.13	15.43	82.44	71.68	148 ± 5
BSO Ar-air dynamic	21	3.14	42.34	140.49	1.42	15.96	82.61	70.46	125 ± 5

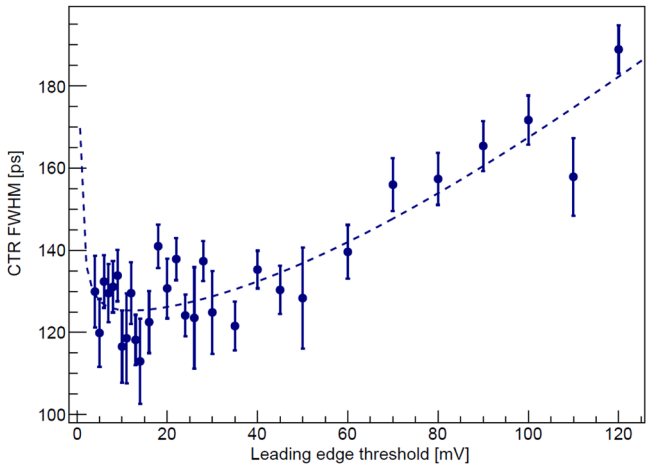

Fig. 8. CTR dependence on the leading edge threshold for the BSO crystal obtained in the Ar-air dynamic atmosphere.

leading to degradation of crystal quality were identified, namely Bi_2O_3 evaporation leading to formation of color centers such as Bi^{3+}- and oxygen vacancies, and Pt inclusions on the crystal surface causing cracks in the bulk. Methods to reduce Pt losses were discussed. Pt inclusions on the crystal surface are caused by crucible surface oxidation below 450 °C, subsequent evaporation of platinum oxides and their dissolution in the melt. Oxygen sources in the growth chamber comprise residual oxygen adsorbed by porous thermal insulation ceramics, and excess oxygen in the raw materials.

A fourfold reduction of Pt losses was achieved by creating the dynamic gas atmosphere in the growth chamber: the crucible was heated to a temperature of 600 °C in Ar, then the chamber was filled with the required amount of air. Since the platinum oxidation process is limited by the oxygen diffusion rate, rapid heating of the crucible to temperatures above 450 °C helped to reduce the thickness of the oxidized platinum layer and minimize Pt losses. In addition, crystallization in air minimized Bi_2O_3 losses due to its evaporation from the melt. As a result, the light output increased by 15 % and the coincidence time resolution improved to 125 ps in the crystal grown in a dynamic Ar-air atmosphere.

Since BSO is an incongruently melting composition crystallized from a Bi_2O_3-enriched melt solution, optimization of Bi_2O_3 excess in the melt is necessary to obtain larger crystals with acceptable optical quality needed for future particle physics experiments. This issue will be addressed in future work.

CRediT authorship contribution statement

Loris Martinazzoli: Writing – review & editing, Investigation, Formal analysis, Data curation, Conceptualization. **Julie Delenne:** Investigation, Data curation. **Pavel Mateychenko:** Methodology, Investigation. **Kateryna Bryleva:** Investigation, Data curation. **Borys Grynyov:** Supervision, Conceptualization. **Oleh Viahin:** Writing – original draft, Investigation, Data curation. **Denys Kofanov:** Investigation, Data curation. **Etiennette Auffray:** Writing – review & editing, Supervision, Project administration, Funding acquisition, Conceptualization. **Iaroslav Gerasymov:** Writing – review & editing, Supervision, Investigation. **Daniil Kurtsev:** Methodology, Investigation. **Louis Roux:** Methodology, Formal analysis, Data curation. **Oleg Sidletskiy:** Writing – original draft, Supervision, Data curation, Conceptualization. **Roberto Cala:** Methodology, Data curation, Conceptualization. **Sergii Tkachenko:** Methodology, Investigation.

Declaration of Competing Interest

all the authors have no conflict of interest to declare.

Acknowledgments

This work was made in the frame of Horizon Europe ERA Widening Project no. 101078960 “TWISMA”. We acknowledge as well the Crystal Clear Collaboration in CERN.

Data availability

Data will be made available on request.

References

[1] B. Adeva, The construction of the L3 experiment, Nuclear Instruments and Methods in Physics Research Section A: Accelerators, Spectrometers, Detectors and Associated Equipment 289 (1990) 35–102. https://doi.org/10.1016/0168-9002(90)90250-A.

[2] P. GianottiThe calorimeters of the PADME experiment, Nuclear Instruments and Methods in Physics Research Section A: Accelerators, Spectrometers, Detectors and Associated Equipment 936 (2019) 150–151. https://doi.org/10.1016/j.nima.2018.09.058.

[3] T.C. Collaboration, S. Chatrchyan, et al., The CMS experiment at the CERN LHC, J. Inst. 3 (2008), https://doi.org/10.1088/1748-0221/3/08/S08004. S08004–S08004.

[4] M. Ishii, K. Harada, Y. Hirose, N. Senguttuvan, M. Kobayashi, I. Yamaga, H. Ueno, K. Miwa, F. Shiji, F. Yiting, M. Nikl, X.Q. Feng, Development of BSO (Bi4Si3O12) crystal for radiation detector, Opt. Mater. 19 (2002) 201–212, https://doi.org/10.1016/S0925-3467(01)00220-8.

[5] R. Cala', N. Kratochwil, L. Martinazzoli, M.T. Lucchini, S. Gundacker, E. Galenin, I. Gerasymov, O. Sidletskiy, M. Nikl, E. AuffrayCharacterization of mixed Bi4(GexSi1−x)3O12 for crystal calorimetry at future colliders, Nuclear Instruments and Methods in Physics Research Section A: Accelerators, Spectrometers, Detectors and Associated Equipment 1032 (2022) 166527. https://doi.org/10.1016/j.nima.2022.166527.

[6] M. Ishii, K. Harada, N. Senguttuvan, M. Kobayashi, I. Yamaga, Crystal growth of BSO (Bi4Si3O12) by vertical Bridgman method, J. Cryst. Growth 205 (1999) 191–195, https://doi.org/10.1016/S0022-0248(99)00232-8.

[7] E. Galenin, M. Biatov, I. Gerasymov, B. Grinyov, O. Sidletskiy, V. Baranov, J. Budagov, Yu Davydov, V. Glagolev, Engineering of mixed Bi4(GexSi1-x)3O12 scintillation crystals, Funct. Mater. 22 (2015) 423–428, https://doi.org/10.15407/fm22.04.423.

[8] V. Vaithianathan, S. Kumaragurubaran, N. Senguttuvan, P. Santhanaraghavan, M. Ishii, P.K. Sinha, P. Ramasamy, Czochralski growth of bismuth germanium silicon oxide (BGSO) single crystal and its characterization, J. Cryst. Growth 235 (2002) 212–216, https://doi.org/10.1016/S0022-0248(01)01725-0.

[9] Y. Zhang, J. Xu, Q. He, B. Lu, Bridgman growth and characterization of Bi4(GexSi1−x)3O12 mixed crystals, J. Cryst. Growth 362 (2013) 121–124, https://doi.org/10.1016/j.jcrysgro.2011.12.088.

[10] V.M. Denisov, O.I. Podkopaev, L.T. Denisova, O.V. Kuchumova, S.A. Istomin, E. A. Pastukhov, Contact interaction of the Bi12GeO20, Bi12SiO20, and Bi4Ge3O12 melts with noble metals, Russ. Metall. 2014 (2014) 97–100, https://doi.org/10.1134/S0036029514020037.

[11] K. Lal, R.V. Anantha Murthy, A. Choubey, N. Goswami, Growth and characterization of technologically important oxide single crystals, in: Crystal Growth Tech., Elsevier, 2003, pp. 387–417, https://doi.org/10.1016/B978-081551453-4.50014-2.

[12] O. Sanz, E. Haro-Poniatowski, J. Gonzalo, J.M.Fernández Navarro, Influence of the melting conditions of heavy metal oxide glasses containing bismuth oxide on their optical absorption, J. Non-Cryst. Solids 352 (2006) 761–768, https://doi.org/10.1016/j.jnoncrysol.2006.02.002.

[13] N. Kinomura, N. Kumada, Preparation of bismuth oxides with mixed valence from hydrated sodium bismuth oxide, Mater. Res. Bull. 30 (1995) 129–134, https://doi.org/10.1016/0025-5408(94)00123-5.

[14] A. Borisov, H. Palme, Experimental determination of the solubility of platinum in silicate melts, Geochim. Et. Cosmochim. Acta 61 (1997) 4349–4357, https://doi.org/10.1016/S0016-7037(97)00268-8.

[15] Fiammetta Pagano, Nicolaus Kratochwil, Isabel Frank, Stefan Gundacker, Marco Paganoni, Marco Pizzichemi, Matteo Salomoni, Etiennette Auffray, A new method to characterize low stopping power and ultra-fast scintillators using pulsed X-rays, Front. Phys. 10 (2022) 1021787, https://doi.org/10.3389/fphy.2022.1021787.

[16] S. Gundacker, R.M. Turtos, E. Auffray, M. Paganoni, P. Lecoq, High-frequency SiPM readout advances measured coincidence time resolution limits in TOF-PET, Phys. Med. Biol. 64 (2019) 055012, https://doi.org/10.1088/1361-6560/aafd52.

[17] J.C. Chaston, Reaction of oxygen with the platinum metals: I—the oxidation of platinum, Platin. Met. Rev. 8 (1964) 50–54, https://doi.org/10.1595/003214064X825054.

[18] P. Arhipov, S. Tkachenko, S. Vasiukov, K. Hubenko, Ia Gerasymov, V. Baumer, A. Puzan, P. Mateychenko, K. Lebbou, O. Sidletskiy, Features of YAG crystal growth under Ar+CO reducing atmosphere, J. Cryst. Growth 449 (2016) 104–107, https://doi.org/10.1016/j.jcrysgro.2016.06.003.

[19] O. Sidletskiy, P. Arhipov, S. Tkachenko, Ia Gerasymov, D. Kurtsev, V. Jarý, R. Kučerková, M. Nikl, K. Lebbou, E. Auffray, Garnet crystal growth in non-

precious metal crucibles, in: M. Korzhik, A. Gektin (Eds.), Engineering of Scintillation Materials and Radiation Technologies, Springer International Publishing, Cham, 2019, pp. 83–95, https://doi.org/10.1007/978-3-030-21970-3_7.

[20] M.V.D.S. Rezende, C.W.A. Paschoal, M.E.G. Valerio, R.A. Jackson, Computer modelling of Bi12SiO20 and Bi4Si3O12: intrinsic defects and rare earth ion incorporation, J. Solid State Chem. 292 (2020) 121608, https://doi.org/10.1016/j.jssc.2020.121608.

[21] A.F. Lima, S.O. Souza, M.V. Lalić, Electronic structure and optical absorption of the Bi4Ge3O12 and the Bi4Si3O12 scintillators in ultraviolet region: an *ab initio* study, J. Appl. Phys. 106 (2009) 013715, https://doi.org/10.1063/1.3160291.

[22] M.E.G. Valerio, R.A. Jackson, Z.S. Macedo, Modelling intrinsic defects and transport mechanisms in the bismuth germanate crystalline system, Phys. Stat. Sol. 2 (2005) 485–489, https://doi.org/10.1002/pssc.200460214.

[23] J. Xu, Y. Pan, T.Tian Ch, H. Mao, Y. Feng, H. Ma, Shao. Effective enhancement of light yield achieved in Bi4Si3O12 scintillation single crystals by doping with tantalum ions, J. Alloy. Compd. 960 (2023) 170754.

[24] J. Hua, H.J. Kim, G. Rooh, H. Park, S. Kim, J. Cheon, Czochralski growth and scintillation properties of Bi4Si3O12 (BSO) single crystal, Nucl. Instrum. Meth. Phys. Res. A 648 (2011) 73–76.